Editors' Suggestion

Constraints on Primordial Gravitational Waves Using *Planck*, WMAP, and New BICEP2/*Keck* Observations through the 2015 Season

P. A. R. Ade,[1] Z. Ahmed,[2] R. W. Aikin,[3] K. D. Alexander,[4] D. Barkats,[4] S. J. Benton,[5] C. A. Bischoff,[6] J. J. Bock,[3,7] R. Bowens-Rubin,[4] J. A. Brevik,[3] I. Buder,[4] E. Bullock,[8] V. Buza,[4,9] J. Connors,[4] J. Cornelison,[4] B. P. Crill,[7] M. Crumrine,[10] M. Dierickx,[4] L. Duband,[11] C. Dvorkin,[9] J. P. Filippini,[12,13] S. Fliescher,[10] J. Grayson,[14] G. Hall,[10] M. Halpern,[15] S. Harrison,[4] S. R. Hildebrandt,[3,7] G. C. Hilton,[16] H. Hui,[3] K. D. Irwin,[14,2,16] J. Kang,[14] K. S. Karkare,[4,17] E. Karpel,[14] J. P. Kaufman,[18] B. G. Keating,[18] S. Kefeli,[3] S. A. Kernasovskiy,[14] J. M. Kovac,[4,9] C. L. Kuo,[14,2] N. A. Larsen,[17] K. Lau,[10] E. M. Leitch,[17] M. Lueker,[3] K. G. Megerian,[7] L. Moncelsi,[3] T. Namikawa,[19] C. B. Netterfield,[20,21] H. T. Nguyen,[7] R. O'Brient,[3,7] R. W. Ogburn IV,[14,2] S. Palladino,[6] C. Pryke,[10,8,*] B. Racine,[4] S. Richter,[4] A. Schillaci,[3] R. Schwarz,[10] C. D. Sheehy,[22] A. Soliman,[3] T. St. Germaine,[4] Z. K. Staniszewski,[3,7] B. Steinbach,[3] R. V. Sudiwala,[1] G. P. Teply,[3,18] K. L. Thompson,[14,2] J. E. Tolan,[14] C. Tucker,[1] A. D. Turner,[7] C. Umiltà,[6] A. G. Vieregg,[23,17] A. Wandui,[3] A. C. Weber,[7] D. V. Wiebe,[15] J. Willmert,[10] C. L. Wong,[4,9] W. L. K. Wu,[17] H. Yang,[14] K. W. Yoon,[14,2] and C. Zhang[3]

(*Keck* Array and BICEP2 Collaborations)

[1]*School of Physics and Astronomy, Cardiff University, Cardiff, CF24 3AA, United Kingdom*
[2]*Kavli Institute for Particle Astrophysics and Cosmology, SLAC National Accelerator Laboratory, 2575 Sand Hill Rd, Menlo Park, California 94025, USA*
[3]*Department of Physics, California Institute of Technology, Pasadena, California 91125, USA*
[4]*Harvard-Smithsonian Center for Astrophysics, 60 Garden Street MS 42, Cambridge, Massachusetts 02138, USA*
[5]*Department of Physics, Princeton University, Princeton, New Jersey 08544, USA*
[6]*Department of Physics, University of Cincinnati, Cincinnati, Ohio 45221, USA*
[7]*Jet Propulsion Laboratory, Pasadena, California 91109, USA*
[8]*Minnesota Institute for Astrophysics, University of Minnesota, Minneapolis, Minnesota 55455, USA*
[9]*Department of Physics, Harvard University, Cambridge, Massachusetts 02138, USA*
[10]*School of Physics and Astronomy, University of Minnesota, Minneapolis, Minnesota 55455, USA*
[11]*Service des Basses Températures, Commissariat à l'Energie Atomique, 38054 Grenoble, France*
[12]*Department of Physics, University of Illinois at Urbana-Champaign, Urbana, Illinois 61801, USA*
[13]*Department of Astronomy, University of Illinois at Urbana-Champaign, Urbana, Illinois 61801, USA*
[14]*Department of Physics, Stanford University, Stanford, California 94305, USA*
[15]*Department of Physics and Astronomy, University of British Columbia, Vancouver, British Columbia, V6T 1Z1, Canada*
[16]*National Institute of Standards and Technology, Boulder, Colorado 80305, USA*
[17]*Kavli Institute for Cosmological Physics, University of Chicago, Chicago, Illinois 60637, USA*
[18]*Department of Physics, University of California at San Diego, La Jolla, California 92093, USA*
[19]*Leung Center for Cosmology and Particle Astrophysics, National Taiwan University, Taipei 10617, Taiwan*
[20]*Department of Physics, University of Toronto, Toronto, Ontario, M5S 1A7, Canada*
[21]*Canadian Institute for Advanced Research, Toronto, Ontario, M5G 1Z8, Canada*
[22]*Physics Department, Brookhaven National Laboratory, Upton, New York 11973, USA*
[23]*Department of Physics, Enrico Fermi Institute, University of Chicago, Chicago, Illinois 60637, USA*

(Received 2 July 2018; revised manuscript received 28 August 2018; published 27 November 2018)

We present results from an analysis of all data taken by the BICEP2/*Keck* CMB polarization experiments up to and including the 2015 observing season. This includes the first *Keck* Array observations at 220 GHz and additional observations at 95 and 150 GHz. The Q and U maps reach depths of 5.2, 2.9, and 26 μK_{CMB} arcmin at 95, 150, and 220 GHz, respectively, over an effective area of ≈400 square degrees. The 220 GHz maps achieve a signal to noise on polarized dust emission approximately equal to that of *Planck* at 353 GHz. We take auto and cross spectra between these maps and publicly available WMAP and *Planck* maps at frequencies from 23 to 353 GHz. We evaluate the joint likelihood of the spectra versus a multicomponent model of lensed-ΛCDM + r + dust + synchrotron + noise. The foreground model has seven parameters, and we impose priors on some of these using external information from *Planck* and WMAP derived from larger regions of sky. The model is shown to be an adequate description of the data at the current noise levels. The likelihood analysis yields the constraint $r_{0.05} < 0.07$ at 95% confidence, which tightens to $r_{0.05} < 0.06$ in conjunction with *Planck* temperature measurements and other data. The lensing

signal is detected at 8.8σ significance. Running a maximum likelihood search on simulations we obtain unbiased results and find that $\sigma(r) = 0.020$. These are the strongest constraints to date on primordial gravitational waves.

DOI: 10.1103/PhysRevLett.121.221301

Introduction.—It is remarkable that our standard model of cosmology, known as ΛCDM, is able to statistically describe the observable Universe with only six parameters (tensions between high and low redshift probes notwithstanding [1]). Observations of the cosmic microwave background (CMB) [2] have played a central role in establishing this model and now constrain these parameters to percent-level precision (see most recently Ref. [3]).

The success of this model focuses our attention on the deep physical mysteries it exposes. Dark matter and dark energy dominate the present-day Universe, but we lack understanding of both their nature and abundance. Perhaps most fundamentally, the standard model offers no explanation for the observed initial conditions of the Universe: highly uniform and flat with small, nearly scale-invariant, adiabatic density perturbations. Inflation is an extension to the standard model that addresses initial conditions by postulating that the observable Universe arose from a tiny, causally connected volume in a period of accelerated expansion within the first fraction of a nanosecond, during which quantum fluctuations of the spacetime metric gave rise to both the observed primordial density perturbations and a potentially observable background of gravitational waves (see Ref. [4] for a recent review and citations to the original literature).

Probing for these primordial gravitational waves through the faint B-mode polarization patterns that they would imprint on the CMB is recognized as one of the most important goals in cosmology today, with the potential to either confirm inflation, and establish its energy scale, or to powerfully limit the space of allowed inflationary models [5]. Multiple groups are making measurements of CMB polarization, some focused on the gravitational wave goal at larger angular scales, and others focused on other science at smaller angular scales; examples include Refs. [6–9].

In principle B-mode polarization patterns offer a unique probe of primordial gravitational waves because they cannot be sourced by primordial density perturbations [10–12]. However, in practice there are two sources of foreground: gravitational deflections of the CMB photons in flight leads to a lensing B-mode component [13], and polarized emission from our own Galaxy can also produce B modes. The latter can be separated out through their differing frequency spectral behavior, so extremely sensitive multifrequency observations are needed to advance the leading constraints on primordial gravitational waves.

Our BICEP/*Keck* program first reported detection of an excess over the lensing B-mode expectation at 150 GHz in Ref. [14]. In a joint analysis using multifrequency data from the *Planck* experiment it was shown that most or all of this is due to polarized emission from dust in our own galaxy [15], hereafter BKP. We first started to diversify our own frequency coverage by adding data taken in 2014 with the *Keck* Array at 95 GHz, yielding the tightest previous constraints on primordial gravitational waves [16], hereafter BK14.

In this Letter (hereafter BK15), we advance these constraints using new data taken by *Keck* Array in the 2015 season including two 95 GHz receivers, a single 150 GHz receiver, and, for the first time, two 220 GHz receivers. This analysis thus doubles the 95 GHz data set from two receiver years to four, while adding a new higher frequency band that significantly improves the constraints on the dust contribution over what is possible using the *Planck* 353 GHz data alone. The constraint on primordial gravitational waves parametrized by tensor to scalar ratio r is improved to $r_{0.05} < 0.062$ (95%), disfavoring the important class of inflationary models represented by a ϕ potential [4,5].

Instrument and observations.—The *Keck* Array consists of a set of five microwave receivers similar in design to the precursor BICEP2 instrument [17,18]. Each receiver employs a ≈0.25 m aperture all cold refracting telescope focusing microwave radiation onto a focal plane of polarized antenna-coupled bolometric detectors [19]. The receivers are mounted on a movable platform (or mount) that scans their pointing direction across the sky in a controlled manner. The detectors are read out through a time-domain multiplexed SQUID readout system. Orthogonally polarized detectors are arranged as coincident pairs in the focal plane, and the pair-difference time stream data thus traces out changes in the polarization signal from place to place on the sky. The telescopes are located at the South Pole in Antarctica where the atmosphere is extremely stable and transparent at the relevant frequencies. The data are recorded to disk and transmitted back to the U.S. daily for analysis.

To date we have mapped a single region of sky centered at RA 0h, Dec. −57.5°. From 2010 to 2013, the BICEP2 and *Keck* Array jointly recorded a total of 13 receiver years of data in a band centered on 150 GHz. Two of the *Keck* receivers were switched to 95 GHz before the 2014 season, and two more were switched to 220 GHz before the 2015 season. The BK15 data set thus consists of 4/17/2 receiver years at 95/150/220 GHz, respectively.

Maps and power spectra.—We make maps and power spectra using the same procedures as used for BK14 and previous analyses [14]. Briefly, the telescope time stream

data are filtered and then binned into sky pixels with the multiple detector pairs being co-added together using knowledge of their individual pointing directions as the telescope scans across the sky. Maps of the polarization Stokes parameters Q and U are constructed by also knowing the polarization sensitivity angle of each pair as projected onto the sky.

After apodizing to downweight the noisy regions around the edge of the observed area, the Q/U maps are Fourier transformed and converted to the E/B basis in which the primordial gravitational wave signal is expected to be maximally distinct from the standard ΛCDM signal.

Two details worth noting are the deprojection of leading order temperature to polarization leakage terms, and the adjustment of the absolute polarization angle to minimize the EB cross spectrum. See Ref. [14] for more information.

For illustration purposes, we can inverse Fourier transform to form E/B maps. Figure 1 shows E-mode maps formed from the 2015 data alone—the data which is being added to the previous data in this analysis. The similarity of the pattern at all three frequencies indicates that ΛCDM

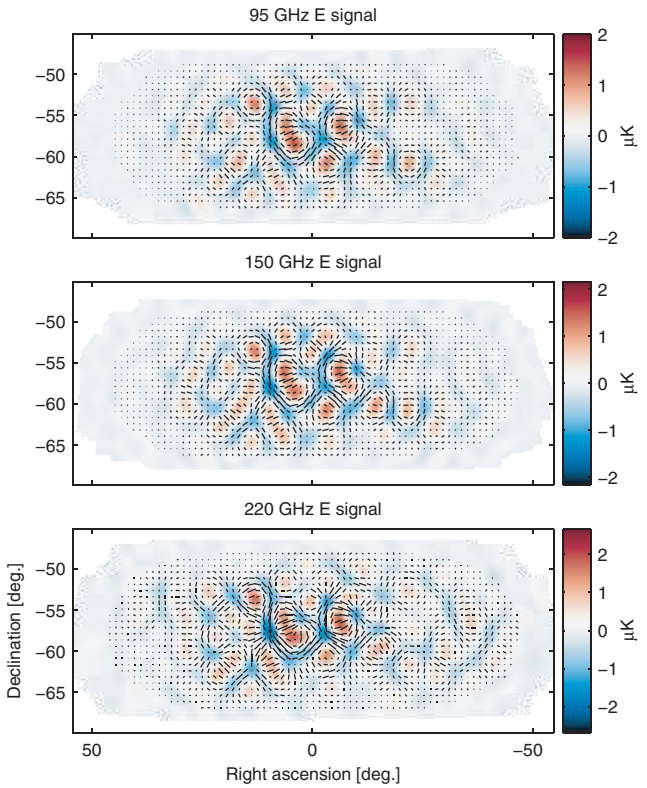

FIG. 1. Maps of degree angular scale E modes ($50 < \ell < 120$) at three frequencies made using *Keck* Array data from the 2015 season only. The similarity of the pattern indicates that ΛCDM E modes dominate at all three frequencies (and that the signal to noise is high). The color scale is in μK, and the range is allowed to vary slightly to (partially) compensate for the decrease in beam size with increasing frequency.

E modes dominate, and that the signal to noise is high. The effective area of these maps is ∼1% of the full sky. (See Appendix A in the Supplemental Material [20] for the full set of $T/Q/U$ maps [20].)

To suppress E to B leakage we use the matrix purification technique which we have developed [14,28]. We then take the variance within annuli of the Fourier plane to estimate the angular power spectra. To test for systematic contamination we carry out our usual "jackknife" internal consistency tests on the new 95 and 220 GHz data as described in Appendices B and C in the Supplemental Material [20]—the distributions of χ and χ^2 PTE values are consistent with uniform showing no evidence for problems.

In this Letter we use the three bands of BICEP2/*Keck* plus the 23 and 33 GHz bands of WMAP [29,30] and all seven polarized bands of *Planck* [31,32]. We take all possible auto- and cross-power spectra between these twelve bands—the full set of spectra are shown in Appendix D in the Supplemental Material [20].

Figure 2 shows the EE and BB auto and cross spectra for the BICEP2/*Keck* bands plus the *Planck* 353 GHz band, which is important for constraining the polarized dust contribution. The spectra are compared to the "baseline" lensed-ΛCDM + dust model from our previous BK14 analysis. Note that the BB spectra involving 220 GHz were not used to derive this model but agree well with it. The EE spectra were also not used to derive the model but agree well with it under the assumption that $EE/BB = 2$ for dust, as it is shown to be close to in the *Planck* analysis of larger regions of sky [33,34]. (Note that many of the BICEP/*Keck* spectra are sample variance dominated.)

Figure 3 (upper panel) shows the noise spectra (derived using the sign-flip technique [14,35]) for the three BK15 bands after correction for the filter and beam suppression. The turn up at low ℓ is partially due to residual atmospheric $1/f$ in the pair-difference data and hence is weakest in the 95 GHz band where water vapor emission is weakest. In an auto spectrum the quantity which determines the ability to constrain r is the fluctuation of the noise band powers rather than their mean. The lower panel therefore shows the effective sky fraction observed as inferred from the fractional noise fluctuation. Together, these panels provide a useful synoptic measure of the loss of information due to noise, filtering, and EE/BB separation in the lowest band powers. We suggest that other experiments reproduce this plot for comparison purposes.

Likelihood analysis.—We perform likelihood analysis using the methods introduced in BKP and refined in BK14. We use the Hamimeche-Lewis (HL) approximation [36] to the joint likelihood of the ensemble of 78 BB auto and cross spectra taken between the BICEP2/*Keck* and WMAP/*Planck* maps. We compare the observed band power values for $20 < \ell < 330$ (9 band powers per spectrum) to an eight parameter model of lensed-ΛCDM$+r+$dust + synchrotron+noise and explore the parameter space

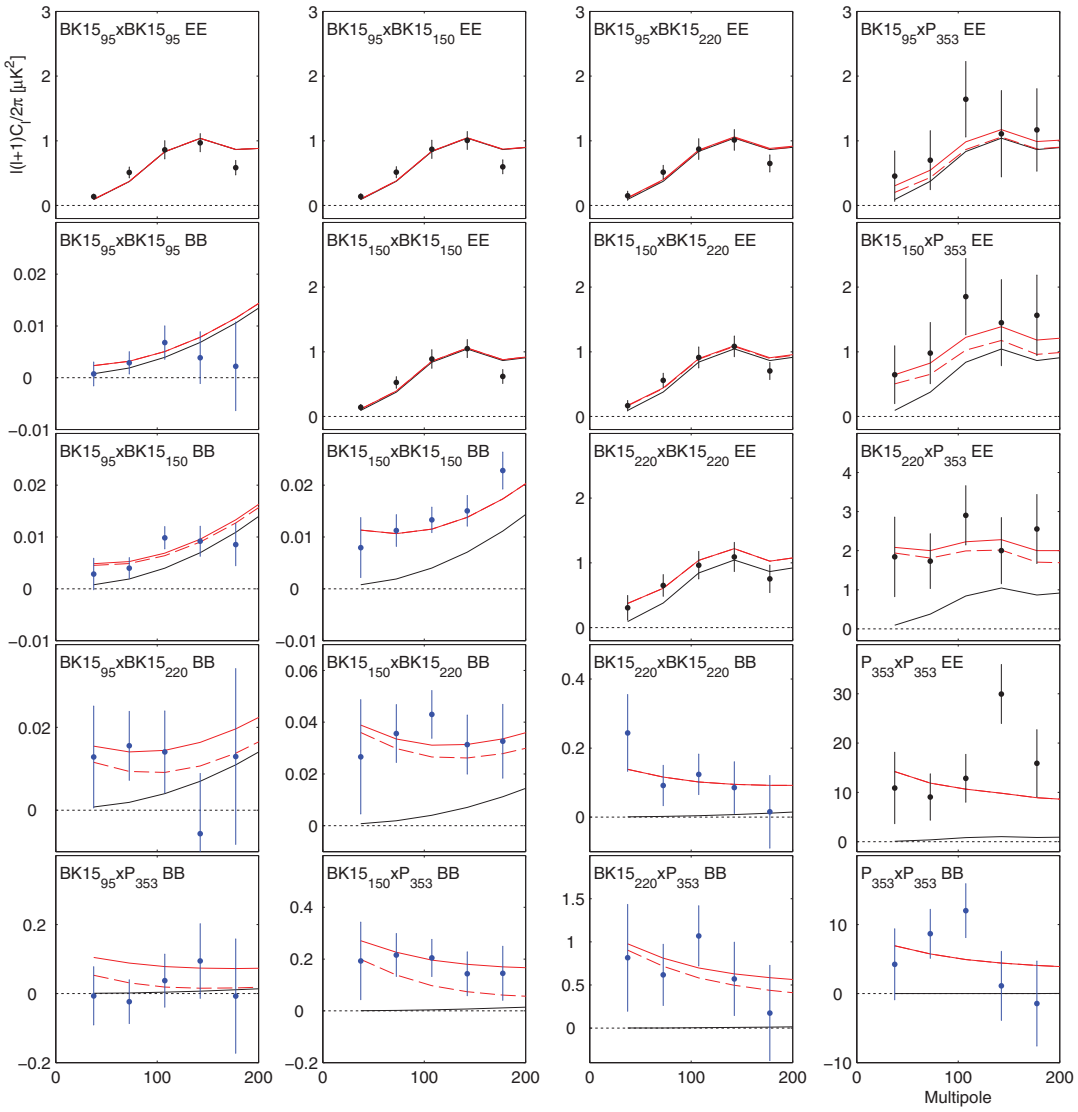

FIG. 2. *EE* and *BB* auto and cross spectra calculated using BICEP2/*Keck* 95, 150, and 220 GHz maps and the *Planck* 353 GHz map. The BICEP2/*Keck* maps use all data taken up to and including the 2015 observing season—we refer to these as BK15. The black lines show the model expectation values for lensed ΛCDM, while the red lines show the expectation values of the baseline lensed-ΛCDM + dust model from our previous BK14 analysis ($r = 0$, $A_{d,353} = 4.3\ \mu\mathrm{K}^2$, $\beta_d = 1.6$, $\alpha_d = -0.4$), and the error bars are scaled to that model. Note that the model shown was fit to *BB* only and did not use the 220 GHz points (which are entirely new). The agreement with the spectra involving 220 GHz and all the *EE* spectra (under the assumption that $EE/BB = 2$ for dust) is therefore a validation of the model. (The dashed red lines show the expectation values of the lensed-ΛCDM + dust model when adding strong spectral decorrelation of the dust pattern—see Appendix F in the Supplemental Material [20] for further information.)

using COSMOMC [37] (which implements a Markov chain Monte Carlo method). As in our previous analyses the band power covariance matrix is derived from 499 simulations of signal and noise, explicitly setting to zero terms such as the covariance of signal-only band powers with noise-only band powers or covariance of BICEP/*Keck* noise band powers with WMAP/*Planck* noise band powers [15]. The tensor to scalar power ratio r is evaluated at a pivot scale of 0.05 Mpc^{-1}, and we fix the tensor spectral index $n_t = 0$. The COSMOMC module containing the data and model is available for download at Ref. [38]. We make only one change to the baseline analysis choices of BK14, expanding the prior on the dust-sync correlation parameter. The following paragraphs briefly summarize.

We include dust with amplitude $A_{d,353}$ evaluated at 353 GHz and $\ell = 80$. The frequency spectral behavior is taken as a modified blackbody spectrum with $T_d = 19.6$ K and $\beta_d = 1.59 \pm 0.11$, using a Gaussian prior with the given 1σ width, this being an upper limit on the patch-to-patch variation [15,39]. We note that the latest *Planck* analysis finds a slightly lower central value of $\beta_d = 1.53$ [34] (well within our prior range) with no detected

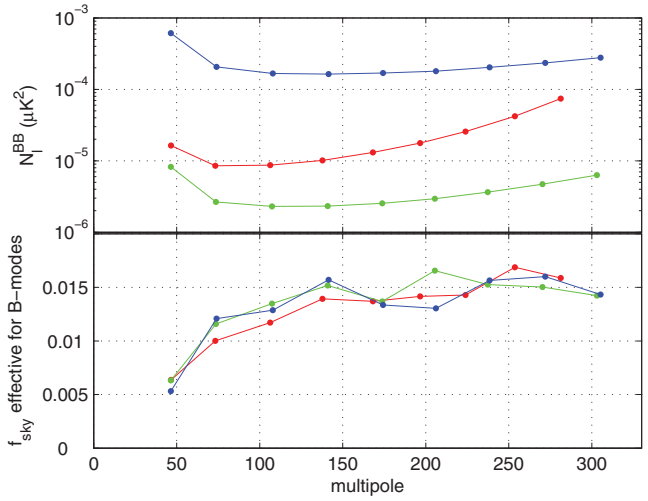

FIG. 3. Upper panel: The noise spectra of the BK15 maps for 95 (red), 150 (green), and 220 GHz (blue) after correction for the filtering of signal, which occurs due to the beam roll-off and time stream filtering. (Note that no ℓ^2 scaling is applied.) Lower panel: The effective sky fraction as calculated from the ratio of the mean noise realization band powers to their fluctuation $f_{\rm sky}(\ell) = (1/2\ell\Delta\ell)[\sqrt{2}\bar{N}_b/\sigma(N_b)]^2$, i.e., the observed number of B mode degrees of freedom divided by the nominal full-sky number. The turn down at low ℓ is due to mode loss to the time stream filtering and matrix purification.

trends with galactic latitude, angular scale, or EE vs BB. The spatial power spectrum is taken as a power law $\mathcal{D}_\ell \propto \ell^{\alpha_d}$ marginalizing uniformly over the (generous) range $-1 < \alpha_d < 0$ [where $\mathcal{D}_\ell \equiv \ell(\ell+1)C_\ell/2\pi$]. *Planck* analysis consistently finds approximate power law behavior of both the EE and BB dust spectra with exponents ≈ -0.4 [33,34].

We include synchrotron with amplitude $A_{\rm sync,23}$ evaluated at 23 GHz (the lowest WMAP band) and $\ell = 80$, assuming a simple power law for the frequency spectral behavior $A_{\rm sync} \propto \nu^{\beta_s}$ with a Gaussian prior $\beta_s = -3.1 \pm 0.3$ [40]. We note that recent analysis of 2.3 GHz data from S-PASS in conjunction with WMAP and *Planck* finds $\beta_s = -3.2$ with no detected trends with galactic latitude or angular scale [41]. The spatial power spectrum is taken as a power law $\mathcal{D}_\ell \propto \ell^{\alpha_s}$ marginalizing over the range $-1 < \alpha_s < 0$ [42]. The recent S-PASS analysis finds a value at the bottom end of this range (≈ -1) for BB at high galactic latitude.

Finally, we include the sync-dust correlation parameter ϵ (called ρ in some other papers [34,41,43]). In BK14 we marginalized over the range $0 < \epsilon < 1$ but in this Letter we extend to the full possible range $-1 < \epsilon < 1$. The latest *Planck* analysis does not detect the sync-dust correlation at high galactic latitude and the ℓ range of interest [34].

Results of the baseline analysis are shown in Fig. 4 and yield the following statistics: $r_{0.05} = 0.020^{+0.021}_{-0.018}$ ($r_{0.05} < 0.072$ at 95% confidence), $A_{d,353} = 4.6^{+1.1}_{-0.9}\,\mu$K^2, and $A_{\rm sync,23} = 1.0^{+1.2}_{-0.8}\,\mu$K^2, ($A_{\rm sync,23} < 3.7\,\mu$K^2 at 95% confidence). For r, the zero-to-peak likelihood ratio is 0.66. Taking $\frac{1}{2}[1 - f(-2\log L_0/L_{\rm peak})]$, where f is the χ^2 CDF (for one degree of freedom), we estimate that the probability to get a likelihood ratio smaller than this is 18% if, in fact, $r = 0$. As compared to the previous analysis, the likelihood curve for r shifts down slightly and tightens. The A_d curve shifts up very slightly but remains about the same width (presumably saturated at sample variance), and the $A_{\rm sync}$ curve loses the second bump at zero.

The maximum likelihood model (including priors) has parameters $r_{0.05} = 0.020$, $A_{d,353} = 4.7\ \mu$K^2, $A_{\rm sync,23} = 1.5\ \mu$K^2, $\beta_d = 1.6$, $\beta_s = -3.0$, $\alpha_d = -0.58$, $\alpha_s = -0.27$, and $\epsilon = -0.38$. This model is an acceptable fit to the data with the probability to exceed (PTE) the observed value of χ^2 being 0.19. Thus, while fluctuation about the assumed power law behavior of the dust component is in general expected to be "super-Gaussian" [34], we find no evidence for this at the present noise level; see Appendix D in the Supplemental Material [20] for further details.

We have explored several variations from the baseline analysis choices and data selection and find that these do not significantly alter the results. Removing the prior on β_d makes the r constraint curve slightly broader resulting in $r_{0.05} < 0.079$ (95%), while using the BICEP/*Keck* data only shifts the peak position down to zero, resulting in $r_{0.05} < 0.063$. Concerns have been raised that the known problems with the LFI maps [44] might affect the analysis—excluding LFI the r constraint curve peak position shifts down to $r = 0.012^{+0.022}_{-0.012}$ ($r_{0.05} < 0.065$, with zero-to-peak likelihood ratio of 0.90, and 32% probability to get a smaller value if $r = 0$), while the constraint on $A_{\rm sync,23}$ becomes $2.4^{+1.9}_{-1.4}\ \mu$K^2. The shifts when varying the data set selection (e.g., omitting *Planck*) are not statistically significant when compared to shifts of lensed-ΛCDM + dust + noise simulations; see Appendices E 1 and E 2 in the Supplemental Material [20] for further details. Freeing the amplitude of the lensing power we obtain $A_L = 1.15^{+0.16}_{-0.14}$, and detect lensing at 8.8σ significance.

The results of likelihood analysis where the parameters are restricted to, and marginalized over, physical values only can potentially be biased. Running the baseline analysis on an ensemble of lensed-ΛCDM + dust + noise simulations with simple Gaussian dust we do not detect bias. Half of the r constraint curves peak at zero and the CDF of the zero-to-peak likelihood ratios closely follows the idealized analytic expectation. When running maximum likelihood searches on the simulations with the parameters unrestricted we again obtain unbiased results and find that $\sigma(r) = 0.020$. See Appendix E 3 in the Supplemental Material [20] for further details.

We extend the maximum likelihood validation study to a suite of third-party foreground models [45–47]. These models do not necessarily conform to the foreground parametrization that we are using, and when fit to it are

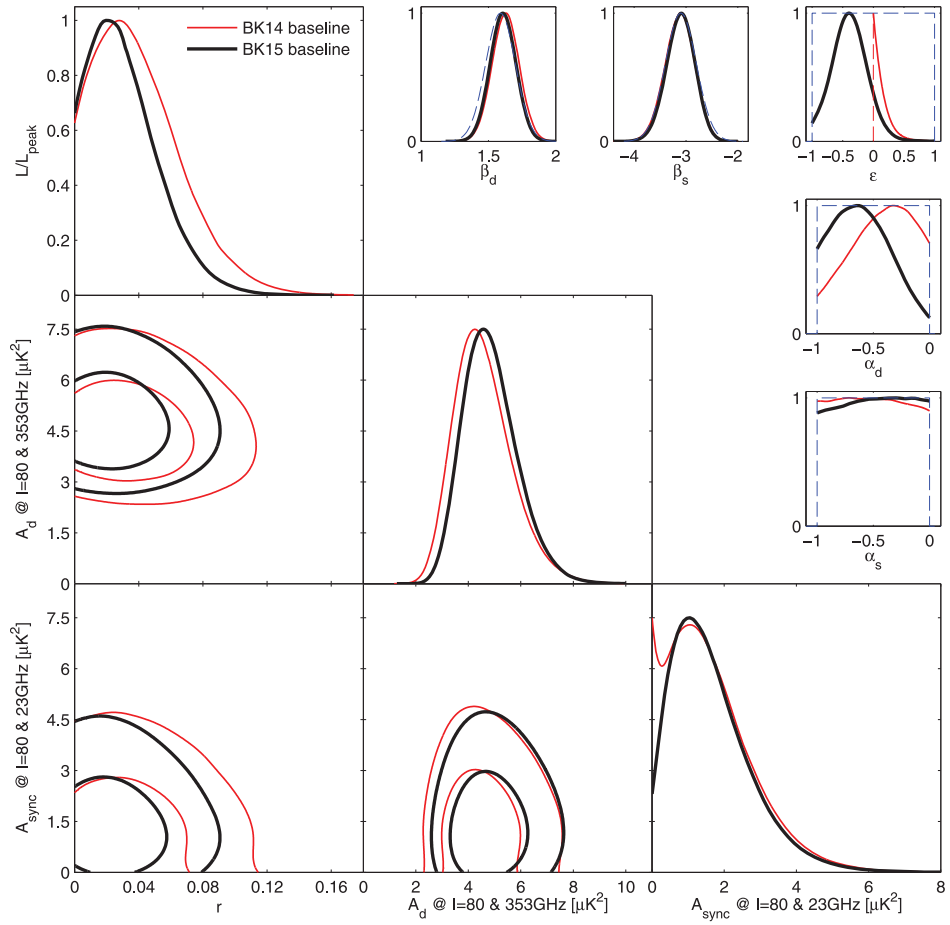

FIG. 4. Results of a multicomponent multispectral likelihood analysis of BICEP2/$Keck$ + WMAP/$Planck$ data. The red faint curves are the baseline result from the previous BK14 paper (the black curves from Fig. 4 of that paper). The bold black curves are the new baseline BK15 results. Differences between these analyses include adding *Keck* Array data taken during the 2015 observing season, in particular doubling the 95 GHz sensitivity and adding, for the first time, a 220 GHz channel. (In addition the ϵ prior is modified.) The upper limit on the tensor-to-scalar ratio tightens to $r_{0.05} < 0.072$ at 95% confidence. The parameters A_d and $A_{\rm sync}$ are the amplitudes of the dust and synchrotron B-mode power spectra, where β and α are the respective frequency and spatial spectral indices. The correlation coefficient between the dust and synchrotron patterns is ϵ. In the β, α, and ϵ panels the dashed lines show the priors placed on these parameters (either Gaussian or uniform). Broadening or tightening the uniform prior range on α_s and α_d results in very small changes, and negligible changes to the r constraint.

in general expected to produce bias on r. However, for the models considered we find that such bias is small compared to the instrumental noise—see Appendix E 4 in the Supplemental Material Ref. [20].

Spatial variation of the frequency spectral behavior of dust will lead to a decorrelation of the dust patterns as observed in different frequency bands. Since the baseline parametric model assumes a fixed dust pattern as a function of frequency such variation will lead to bias on r. Dust decorrelation surely exists at some level—the question is whether it is relevant as compared to the current experimental noise. For the third-party foreground models mentioned above, decorrelation is very small. Since our previous BK14 paper, *Planck* Intermediate Paper L [48] appeared claiming a detection of relatively strong dust decorrelation between 217 and 353 GHz. This was followed up by Ref. [49], which analyzed the same data and found no evidence for dust decorrelation, and *Planck* Intermediate Paper LIV [34], which performed a more sophisticated multifrequency analysis and again found no evidence. In the meantime, we added a decorrelation parameter to our analysis framework. Including it only increases $\sigma(r)$ from 0.020 to 0.021, but for the present data set this parameter is partially degenerate with r and including it results in a downward bias on r in simulations—see Appendix F in the Supplemental Material [20] for more details.

By cross correlating against the *Planck* CO map we find that the contamination of our 220 GHz map by CO is equivalent to $r \sim 10^{-4}$.

Conclusions.—The previous BK14 analysis yielded the constraint $r_{0.05} < 0.090$ (95%). Adding the *Keck* Array data taken during 2015 we obtain the BK15 result

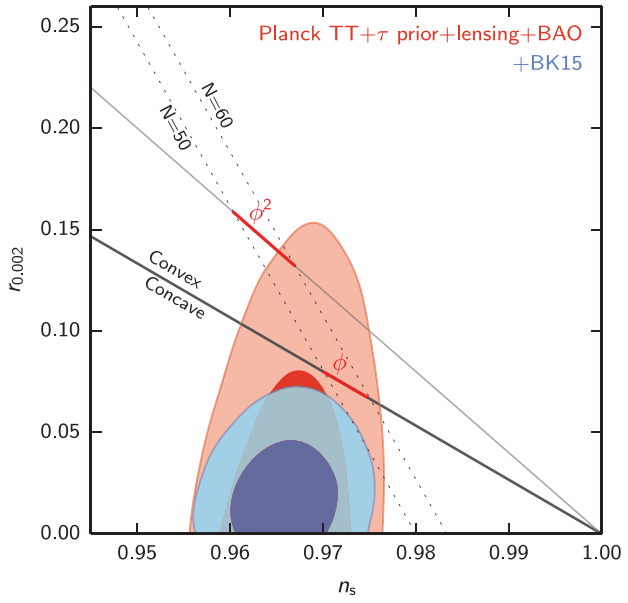

FIG. 5. Constraints in the r vs n_s plane when using *Planck* 2015 plus additional data, and when also adding BICEP2/*Keck* data through the end of the 2015 season—the constraint on r tightens from $r_{0.05} < 0.12$ to $r_{0.05} < 0.06$. This figure is adapted from Fig. 21 of Ref. [3], with two notable differences: switching *lowP* to *lowT* plus a τ prior of 0.055 ± 0.009 Ref. [50], and the exclusion of JLA data and the H_0 prior.

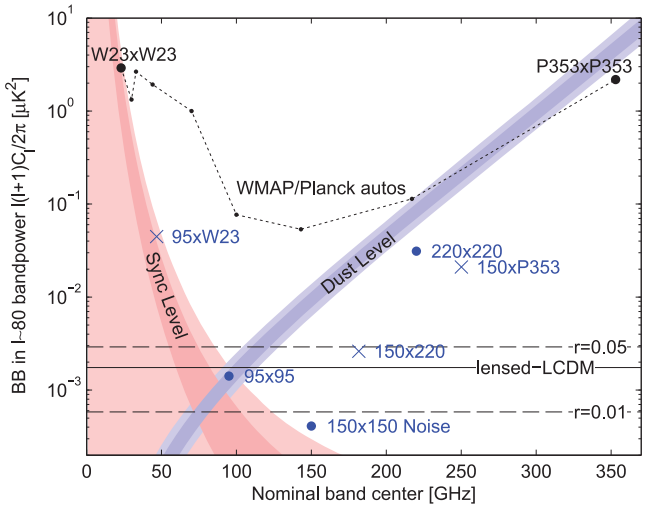

FIG. 6. Expectation values and noise uncertainties for the $\ell \sim 80$ *BB* band power in the BICEP2/*Keck* field. The solid and dashed black lines show the expected signal power of lensed-ΛCDM and $r_{0.05} = 0.05$ and 0.01. Since CMB units are used, the levels corresponding to these are flat with frequency. The blue and red bands show the 1 and 2σ ranges of dust and synchrotron in the baseline analysis including the uncertainties in the amplitude and frequency spectral index parameters ($A_{\mathrm{sync},23}$, β_s, and $A_{d,353}$, β_d). The BICEP2/*Keck* auto-spectrum noise uncertainties are shown as large blue circles, and the noise uncertainties of the WMAP/*Planck* single-frequency spectra evaluated in the BICEP2/*Keck* field are shown in black. The blue crosses show the noise uncertainty of selected cross spectra, and are plotted at horizontal positions such that they can be compared vertically with the dust and sync curves.

$r_{0.05} < 0.072$. The distributions of maximum likelihood r values in simulations where the true value of r is zero give $\sigma(r_{0.05}) = 0.024$ and $\sigma(r_{0.05}) = 0.020$ for BK14 and BK15, respectively. The BK15 simulations have a median 95% upper limit of $r_{0.05} < 0.046$.

Figure 5 shows the constraints in the r vs n_s plane for *Planck* 2015 plus additional data ($r_{0.05} < 0.12$) and when adding in also BK15 ($r_{0.05} < 0.062$). In contrast to the BK14 result the ϕ model now lies entirely outside of the 95% contour.

Figure 6 shows the BK15 noise uncertainties in the $\ell \approx 80$ band powers as compared to the signal levels. Note that the new *Keck* 220 GHz band has approximately the same signal-to-noise on dust as *Planck* 353 GHz with two receiver years of operation. In 2016 and 2017 we recorded an additional eight receiver-years of data which will reduce the noise by a factor of 5 & $\sqrt{5}$ for 220×220 and 150×220, respectively.

As seen in the lower right panel of Fig. 4 with four *Keck* receiver years of data, our 95 GHz data start to weakly prefer a nonzero value for the synchrotron amplitude for the first time. In 2017 alone BICEP3 recorded nearly twice as much data in the 95 GHz band as is included in the current result. We plan to proceed directly to a BK17 result, which can be expected to improve substantially on the current results.

Dust decorrelation, and foreground complexity more generally, will remain a serious concern. With higher quality data we will be able to constrain the foreground behavior ever better, but of course we will also need to constrain it ever better. The BICEP Array experiment that is under construction will provide BICEP3 class receivers in the 30/40, 95, 150, and 220/270 GHz bands and is projected to reach $\sigma(r) < 0.005$ within five years.

The BICEP2/*Keck* Array projects have been made possible through a series of grants from the National Science Foundation including No. 0742818, No. 0742592, No. 1044978, No. 1110087, No. 1145172, No. 1145143, No. 1145248, No. 1639040, No. 1638957, No. 1638978, and No. 1638970, and by the *Keck* Foundation. The development of antenna-coupled detector technology was supported by the JPL Research and Technology Development Fund, and by NASA Grants No. 06-ARPA206-0040, No. 10-SAT10-0017, No. 12-SAT12-0031, No. 14-SAT14-0009, No. 16-SAT-16-0002. The development and testing of focal planes were supported by the Gordon and Betty Moore Foundation at Caltech. Readout electronics were supported by a Canada Foundation for Innovation grant to UBC. Support for quasi-optical filtering was provided by UK STFC Grant No. ST/N000706/1. The computations in this Letter were run on the Odyssey cluster supported by the FAS Science Division

Research Computing Group at Harvard University. The analysis effort at Stanford and S. L. A. C. is partially supported by the U.S. DOE Office of Science. We thank the staff of the U.S. Antarctic Program and in particular the South Pole Station without whose help this research would not have been possible. Most special thanks go to our heroic winterovers Robert Schwarz and Steffen Richter. We thank all those who have contributed past efforts to the BICEP-*Keck* Array series of experiments, including the BICEP1 team. We also thank the *Planck* and WMAP teams for the use of their data, and are grateful to the *Planck* team for helpful discussions including on the use of the τ prior in Fig. 5.

*pryke@physics.umn.edu

[1] N. Aghanim *et al.* (Planck Collaboration), Planck 2018 results. VI. Cosmological parameters, arXiv:1807.06209.
[2] A. A. Penzias and R. W. Wilson, A measurement of excess antenna temperature at 4080 Mc/s, Astrophys. J. **142**, 419 (1965).
[3] P. A. R. Ade *et al.* (Planck Collaboration), Planck 2015 results. XIII. Cosmological parameters, Astron. Astrophys. **594**, A13 (2016).
[4] M. Kamionkowski and E. D. Kovetz, The quest for B modes from inflationary gravitational waves, Annu. Rev. Astron. Astrophys. **54**, 227 (2016).
[5] K. N. Abazajian *et al.*, CMB-S4 Science Book, First Edition, arXiv:1610.02743.
[6] R. Keisler *et al.*, Measurements of sub-degree B-mode polarization in the cosmic microwave background from 100 square degrees of SPTPOL data, Astrophys. J. **807**, 151 (2015).
[7] T. Louis *et al.*, The Atacama Cosmology Telescope: Two-season ACTPol spectra and parameters, J. Cosmol. Astropart. Phys. 06 (2017) 031.
[8] P. A. R. Ade *et al.* (POLARBEAR Collaboration), A measurement of the cosmic microwave background B-mode polarization power spectrum at subdegree scales from two years of POLARBEAR data, Astrophys. J. **848**, 121 (2017).
[9] A. Kusaka *et al.*, Results from the Atacama B-mode Search (ABS) experiment, J. Cosmol. Astropart. Phys. 09 (2018) 005.
[10] U. Seljak, Measuring polarization in the cosmic microwave background, Astrophys. J. **482**, 6 (1997).
[11] M. Kamionkowski, A. Kosowsky, and A. Stebbins, A Probe of Primordial Gravity Waves and Vorticity, Phys. Rev. Lett. **78**, 2058 (1997).
[12] U. Seljak and M. Zaldarriaga, Signature of Gravity Waves in the Polarization of the Microwave Background, Phys. Rev. Lett. **78**, 2054 (1997).
[13] M. Zaldarriaga and U. Seljak, Gravitational lensing effect on cosmic microwave background polarization, Phys. Rev. D **58**, 023003 (1998).
[14] P. A. R. Ade *et al.* (BICEP2 Collaboration), Detection of B-Mode Polarization at Degree Angular Scales by BICEP2, Phys. Rev. Lett. **112**, 241101 (2014).
[15] P. A. R. Ade *et al.* (BICEP2/Keck and Planck Collaborations), Joint Analysis of BICEP2/Keck Array and Planck Data, Phys. Rev. Lett. **114**, 101301 (2015).
[16] P. A. R. Ade *et al.* (Keck Array and BICEP2 Collaborations), Improved Constraints on Cosmology and Foregrounds from BICEP2 and Keck Array Cosmic Microwave Background Data with Inclusion of 95 GHz Band, Phys. Rev. Lett. **116**, 031302 (2016).
[17] P. A. R. Ade *et al.* (BICEP2 Collaboration), BICEP2. II. Experiment and three-year data set, Astrophys. J. **792**, 62 (2014).
[18] P. A. R. Ade *et al.* (Keck Array and BICEP2 Collaborations), BICEP2/Keck array V: Measurements of B-mode polarization at degree angular scales and 150 GHz by the Keck array, Astrophys. J. **811**, 126 (2015).
[19] P. A. R. Ade *et al.* (BICEP2, Keck Array, and SPIDER Collaborations), Antenna-coupled TES bolometers used in BICEP2, Keck array, and spider, Astrophys. J. **812**, 176 (2015).
[20] See Supplemental Material at http://link.aps.org/supplemental/10.1103/PhysRevLett.121.221301 for Appendices, which include Refs. [21–27].
[21] P. A. R. Ade *et al.* (Keck Array and BICEP2 Collaborations), BICEP2/Keck Array XI: Beam Characterization and Temperature-to-Polarization Leakage in the BK15 Dataset (to be published).
[22] R. Adam *et al.* (Planck Collaboration), Planck 2015 results. X. Diffuse component separation: Foreground maps, Astron. Astrophys. **594**, A10 (2016).
[23] D. P. Finkbeiner, M. Davis, and D. J. Schlegel, Extrapolation of galactic dust emission at 100 microns to cosmic microwave background radiation frequencies using FIRAS, Astrophys. J. **524**, 867 (1999).
[24] F. Vansyngel, F. Boulanger, T. Ghosh, B. D. Wandelt, J. Aumont, A. Bracco, F. Levrier, P. G. Martin, and L. Montier, Statistical simulations of the dust foreground to cosmic microwave background polarization, Astron. Astrophys. **603**, A62 (2017).
[25] P. A. R. Ade *et al.* (Planck Collaboration), Planck 2013 results. IX. HFI spectral response, Astron. Astrophys. **571**, A9 (2014).
[26] P. A. R. Ade *et al.* (Keck Array and BICEP2 Collaborations), BICEP2/Keck array VIII: Measurement of gravitational lensing from large-scale B-mode polarization, Astrophys. J. **833**, 228 (2016).
[27] P. A. R. Ade *et al.* (Planck Collaboration), Planck 2015 results. XV. Gravitational lensing, Astron. Astrophys. **594**, A15 (2016).
[28] P. A. R. Ade *et al.* (Keck Array and BICEP2 Collaborations), BICEP2/Keck array. VII. Matrix based E/B separation applied to BICEP2 and the Keck array, Astrophys. J. **825**, 66 (2016).
[29] See http://lambda.gsfc.nasa.gov/product/map/dr5/m_products.cfm.
[30] C. L. Bennett *et al.*, Nine-year Wilkinson Microwave Anisotropy Probe (WMAP) observations: Final maps and results, Astrophys. J. Suppl. Ser. **208**, 20 (2013).
[31] Public Release 2 "full mission" maps as available at http://www.cosmos.esa.int/web/planck/pla. We will update to PR3 in our next analysis.

[32] R. Adam *et al.* (Planck Collaboration), Planck 2015 results. I. Overview of products and scientific results, Astron. Astrophys. **594**, A1 (2016).
[33] R. Adam *et al.* (Planck Collaboration), Planck intermediate results. XXX. The angular power spectrum of polarized dust emission at intermediate and high Galactic latitudes, Astron. Astrophys. **586**, A133 (2016).
[34] Y. Akrami *et al.* (Planck Collaboration), Planck 2018 results. XI. Polarized dust foregrounds, arXiv:1801.04945.
[35] A. van Engelen *et al.*, A measurement of gravitational lensing of the microwave background using South Pole Telescope data, Astrophys. J. **756**, 142 (2012).
[36] S. Hamimeche and A. Lewis, Likelihood analysis of CMB temperature and polarization power spectra, Phys. Rev. D **77**, 103013 (2008).
[37] A. Lewis and S. Bridle, Cosmological parameters from CMB and other data: A Monte Carlo approach, Phys. Rev. D **66**, 103511 (2002).
[38] http://bicepkeck.org.
[39] P. A. R. Ade *et al.* (Planck Collaboration), Planck intermediate results. XXII. Frequency dependence of thermal emission from Galactic dust in intensity and polarization, Astron. Astrophys. **576**, A107 (2015).
[40] U. Fuskeland, I. K. Wehus, H. K. Eriksen, and S. K. Næss, Spatial variations in the spectral index of polarized synchrotron emission in the 9 yr WMAP Sky maps, Astrophys. J. **790**, 104 (2014).
[41] N. Krachmalnicoff, E. Carretti, C. Baccigalupi, G. Bernardi, S. Brown, B. M. Gaensler, M. Haverkorn, M. Kesteven, F. Perrotta, S. Poppi, and L. Staveley-Smith, The S-PASS view of polarized Galactic Synchrotron at 2.3 GHz as a contaminant to CMB observations, arXiv:1802.01145.
[42] J. Dunkley *et al.*, Prospects for polarized foreground removal, AIP Conf. Proc. **1141**, 222 (2009).
[43] S. K. Choi and L. A. Page, Polarized galactic synchrotron and dust emission and their correlation, J. Cosmol. Astropart. Phys. 12 (2015) 020.
[44] P. A. R. Ade *et al.* (Planck Collaboration), Planck 2015 results. II. Low Frequency Instrument data processings, Astron. Astrophys. **594**, A2 (2016).
[45] B. Thorne, J. Dunkley, D. Alonso, and S. Næss, The Python Sky Model: Software for simulating the Galactic microwave sky, Mon. Not. R. Astron. Soc. **469**, 2821 (2017).
[46] B. Hensley, On the nature of interstellar grains, Ph.D. thesis, Princeton University, 2015.
[47] A. G. Kritsuk, S. D. Ustyugov, and M. L. Norman, The structure and statistics of interstellar turbulence, New J. Phys. **19**, 065003 (2017).
[48] P. A. R. Ade *et al.* (Planck Collaboration), Planck intermediate results. L. Evidence of spatial variation of the polarized thermal dust spectral energy distribution and implications for CMB *B*-mode analysis, Astron. Astrophys. **599**, A51 (2017).
[49] C. Sheehy and A. Slosar, No evidence for dust *B*-mode decorrelation in Planck data, Phys. Rev. D **97**, 043522 (2018).
[50] N. Aghanim *et al.* (Planck Collaboration), Planck intermediate results. XLVI. Reduction of large-scale systematic effects in HFI polarization maps and estimation of the reionization optical depth, Astron. Astrophys. **596**, A107 (2016).